

Current carrying states in the disordered quantum anomalous Hall effect

Yi-Ming Dai(戴镒明), Si-Si Wang(王思思), Yan Yu(禹言), Ji-Huan Guan(关济寰), Hui-Hui Wang(王慧慧), and Yan-Yang Zhang(张艳阳)

Citation: Chin. Phys. B, 2022, 31 (**9**): 097302. DOI: 10.1088/1674-1056/ac5d2b
Journal homepage: http://cpb.iphy.ac.cn; http://iopscience.iop.org/cpb

What follows is a list of articles you may be interested in

Floquet topological phase transition in two-dimensional quadratic band crossing system

Guo-Bao Zhu(朱国宝) and Hui-Min Yang(杨慧敏)
Chin. Phys. B, 2021, 30 (**6**): 067304. DOI: 10.1088/1674-1056/abdda4

Quantum anomalous Hall effect in real materials

Jiayong Zhang(张加永), Bao Zhao(赵宝), Tong Zhou(周通), Zhongqin Yang(杨中芹)
Chin. Phys. B, 2016, 25 (**11**): 117308. DOI: 10.1088/1674-1056/25/11/117308

AlO_x/LiF composite protection layer for Cr-doped (Bi, Sb)$_2$Te$_3$ quantum anomalous Hall films

Yunbo Ou(欧云波), Yang Feng(冯洋), Xiao Feng(冯硝), Zhenqi Hao(郝镇齐), Liguo Zhang(张立果), Chang Liu(刘畅), Yayu Wang(王亚愚), Ke He(何珂), Xucun Ma(马旭村), Qikun Xue(薛其坤)
Chin. Phys. B, 2016, 25 (**8**): 087307. DOI: 10.1088/1674-1056/25/8/087307

Silicene on substrates: A theoretical perspective

Zhong Hong-Xia, Quhe Ru-Ge, Wang Yang-Yang, Shi Jun-Jie, Lü Jin
Chin. Phys. B, 2015, 24 (**8**): 087308. DOI: 10.1088/1674-1056/24/8/087308

From magnetically doped topological insulator to the quantum anomalous Hall effect

He Ke, Ma Xu-Cun, Chen Xi, Lü Li, Wang Ya-Yu, Xue Qi-Kun
Chin. Phys. B, 2013, 22 (**6**): 067305. DOI: 10.1088/1674-1056/22/6/067305

Current carrying states in the disordered quantum anomalous Hall effect

Yi-Ming Dai(戴镒明)[1,2], Si-Si Wang(王思思)[1,2,3], Yan Yu(禹言)[4,5], Ji-Huan Guan(关济寰)[6,4], Hui-Hui Wang(王慧慧)[1,7,2], and Yan-Yang Zhang(张艳阳)[1,7,2,3,†]

[1] *School of Physics and Materials Science, Guangzhou University, Guangzhou* 510006, *China*
[2] *Research Center for Advanced Information Materials, Guangzhou University, Guangzhou* 510006, *China*
[3] *School of Mathematics and Information Science, Guangzhou University, Guangzhou* 510006, *China*
[4] *SKLSM, Institute of Semiconductors, Chinese Academy of Sciences, Beijing* 100083, *China*
[5] *School of Physical Sciences, University of Chinese Academy of Sciences, Beijing* 100049, *China*
[6] *Beijing Academy of Quantum Information Sciences, Beijing* 100193, *China*
[7] *Huangpu Research and Graduate School of Guangzhou University, Guangzhou* 510700, *China*

(Received 13 January 2022; revised manuscript received 4 March 2022; accepted manuscript online 14 March 2022)

In a quantum Hall effect, flat Landau levels may be broadened by disorder. However, it has been found that in the thermodynamic limit, all extended (or current carrying) states shrink to one single energy value within each Landau level. On the other hand, a quantum anomalous Hall effect consists of dispersive bands with finite widths. We numerically investigate the picture of current carrying states in this case. With size scaling, the spectrum width of these states in each bulk band still shrinks to a single energy value in the thermodynamic limit, in a power law way. The magnitude of the scaling exponent at the intermediate disorder is close to that in the quantum Hall effects. The number of current carrying states obeys similar scaling rules, so that the density of states of current carrying states is finite. Other states in the bulk band are localized and may contribute to the formation of a topological Anderson insulator.

Keywords: quantum anomalous Hall effect, Chern number, disordered system, localization

PACS: 73.20.Fz, 73.43.–f, 74.62.En **DOI:** 10.1088/1674-1056/ac5d2b

1. Introduction

A Chern insulator is a two-dimensional (2D) material without time reversal symmetry, whose occupied bands possess a nonzero Chern number.[1,2] This Chern number gives rise to topological edge states in the bulk gap, leading to robust transports against weak disorder. The earliest example is the integer quantum Hall (IQH) effect in an external magnetic field, where energy bands are flat and highly degenerate Landau levels.[3] Disorder introduces localized states and broadens Landau levels. Taking states associated with nonzero Chern number as current carrying (CC) or delocalized states, previous numerical studies show that in the thermodynamic limit, these CC states shrink into one single energy value in each disorder broadened Landau level.[4–7] In the presence of a random magnetic field, it takes some endeavors to understand that a similar picture holds.[7–9]

Quantum anomalous Hall (QAH) effect corresponds to a Chern insulator without an external magnetic field, which was firstly proposed by Haldane[10] and realized in recent years.[11–15] In the clean limit, instead of flat Landau levels in IQH systems, the energy bands of a QAH system are dispersive and with finite widths. With increasing disorder, the global route towards localization of QHE effects in the transport picture has been investigated extensively.[16–19] Very recent researches shed light on the difference of localization between QAH and IQH effects.[19,20] However, a detailed picture of CC states is not clear so far, for example, their distributions and evolutions under increasing disorder. Moreover, at weak disorder, will the spectrum width of CC states within each dispersive bulk band still vanish in the thermodynamic limit?

To resolve these issues, in this manuscript, we perform a numerical investigation on a disordered two-band QHA lattice model with Chern number 1. Based on a real space method of evaluating Chern numbers, we study the picture of CC states before localization through size scaling. We find that, in spite of dispersive bulk bands with finite width, the CC states also shrink into a single energy value in the thermodynamic limit. The rate of shrinking during size scaling depends on the disorder strength. At the intermediate disorder, it is equal to that found in the IQH effect.[4]

2. Model and method

We adopt the spin-up component of the Bernevig–Hughes–Zhang (BHZ) model.[21] With broken time reversal symmetry, it is a model of QAH effect,[22] which has been realized in a qubit based synthetic structure recently.[23] It is defined on a square lattice with two orbitals on each site. This spinless Hamiltonian has the form as $\mathcal{H} =$

†Corresponding author. E-mail: yanyang@gzhu.edu.cn
© 2022 Chinese Physical Society and IOP Publishing Ltd

$\sum_{\boldsymbol{k},\alpha\beta} c^{\dagger}_{\boldsymbol{k}\alpha} H_{\alpha\beta}(\boldsymbol{k}) c_{\boldsymbol{k}\beta}$, where $c^{\dagger}_{\boldsymbol{k}\alpha}$ ($c_{\boldsymbol{k}\alpha}$) creates (annihilates) an electron with wavevector $\boldsymbol{k} \equiv (k_x, k_y)$ and orbital $\alpha \in \{1,2\}$. The 2×2 matrix $H_{\alpha\beta}(\boldsymbol{k})$ reads

$$H(\boldsymbol{k}) = d_0(\boldsymbol{k}) I_{2\times 2} + \sum_{i=1}^{3} d_i(\boldsymbol{k})\sigma_i, \tag{1}$$

$$\begin{aligned} d_0(\boldsymbol{k}) &= -2D\big[2-\cos(k_x)-\cos(k_y)\big], \\ d_1(\boldsymbol{k}) &= A\sin(k_x), \quad d_2(\boldsymbol{k}) = A\sin(k_y), \\ d_3(\boldsymbol{k}) &= M - 2B\big[2-\cos(k_x)-\cos(k_y)\big], \end{aligned} \tag{2}$$

where σ_i are Pauli matrices acting on the orbital space.

When the Fermi energy is in the bulk gap $(-|M|, |M|)$, the system is in the QAH state with Chern number 1 if $B\cdot M > 0$. In this paper we adopt the following model parameters $A = 0.3$, $B = 0.2$, $D = 0$, and $M = 0.2$, making a bulk gap region $(-0.2, 0.2)$.

The real space representation of the Hamiltonian $\sum_{ij,\alpha\beta} c^{\dagger}_{i\alpha} H_{\alpha\beta}(i,j) c_{j\beta}$ can be yielded by a straightforward inverse Fourier transformation, where i and j are indices for lattice sites (also unit cells here). The lattice constant $a = 1$ is used as the length unit. The band structure of a ribbon geometry is shown in Fig. 1(a). In the bulk gap, a pair of edge states (red lines) can be clearly seen, for which the left-going (right-going) branch travels on the upper (lower) edge of the ribbon, respectively.[21,24] They originate from Chern number 1 of the occupied states, which is a typical manifestation of the bulk–edge correspondence of Chern insulators.[25]

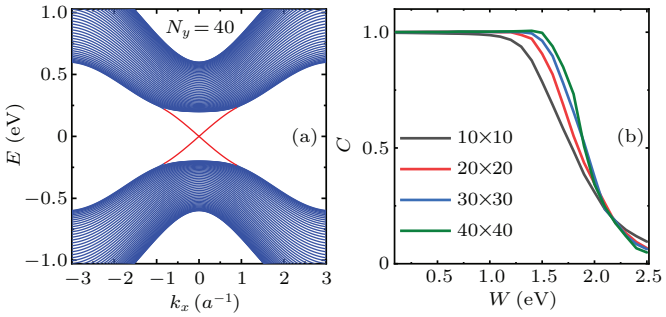


Fig. 1. (a) The band structure of a ribbon geometry with width $N_y = 40$ and open boundary condition. (b) Chern number at Fermi energy $\mu = 0$ as a function of disorder strength W, for different sample sizes $N_x \times N_x$. All data are averaged over at least 100 disorder configurations. The model parameters are: $A = 0.3$, $B = 0.2$, $D = 0$, $M = 0.2$, which will be used throughout this manuscript.

In real space, the effect of disorder is included as a random potential term to the Hamiltonian as

$$V_{\mathrm{I}} = \sum_{i\alpha} W U_i c^{\dagger}_{i\alpha} c_{i\alpha}, \tag{3}$$

where U_i are independent random numbers uniformly distributed in $(-0.5, 0.5)$ and W is the disorder strength.

Topological invariants are usually conveniently defined in the momentum space.[1,2,24,26,27] However here, disorder destroys the translation invariant symmetry. Therefore it is more convenient to investigate this problem in the real space. For a disordered finite-size system, our evaluation of Chern numbers is based on the real space algorithm of the topological marker at position $\boldsymbol{r} = (x, y)$ and Fermi energy μ[28,29]

$$C(\boldsymbol{r}) = 4\pi \mathrm{Im}\langle \boldsymbol{r}|QxPyQ|\boldsymbol{r}\rangle, \tag{4}$$

where $P = \sum_{\varepsilon_n<\mu} |\psi_n\rangle\langle\psi_n|$ is the projector over occupied eigenstates $\{|\psi_n\rangle\}$ of the Hamiltonian, and $Q = 1 - P$. It has been argued that its value at the sample center tends to be the Chern number at thermodynamic limit.[29,30] Taking each energy level as the Fermi level one by one, we can associate a quantized Chern number to each level based on reasonable considerations. Details of this calculation are described in the Appendix. Following previous spirits and definitions in Refs. [4,5,7,31], we take the eigenstates associated with nonzero Chern numbers as CC states, which play the role as delocalized states. Then, the Chern number resolved density of states (DOS) is defined to be[4,31]

$$\rho_C(E) = \sum_{n\in\{\text{levels associated with } C\}} \delta(E - E_n), \tag{5}$$

where the sum is over energy levels associated with the same Chern number C. Hereafter in this manuscript, all finite samples are square shaped with lattice sites $N \equiv N_x \times N_x$.

For a Chern number resolved DOS, the spectrum width ΔE along the energy axis is a key property. In the pioneer work,[4] this was defined as the standard deviation of the energy level distribution. This was suitable there because their calculations were strictly restricted within the lowest Landau level alone.[4] Here however, we are facing a lattice model with two bands, and disorder may generate more subbands as sub-peaks of DOS [see, e.g., Fig. 3(b)]. In this case, the standard deviation over the whole energy is not a good definition as ΔE of a certain band or peak, since far sub-peaks will contribute remarkable but unwanted standard deviation. Instead, we adopt the width at half height of the main peak as the spectrum width ΔE here.

3. Results

In Fig. 1(b), we plot the disorder averaged Chern number C as a function of disorder strength W, for different sample sizes $N \equiv N_x \times N_x$, which is evaluated at Fermi energy $\mu = 0$. Here and in the rest of this paper, we check the convergence of the averaging by adopting sufficiently number of disorder samples, which is the most time consuming part of this work. The Chern number is a well quantized plateau when $W \lesssim 1$, reflecting the robustness of a topological phase against weak disorder. We call this range the Chern number plateau region. After that, the quantization starts to collapse successively, at a larger W for a larger size. Finally strong disorder leads the system towards an Anderson localization with $C = 0$ after $W \gtrsim 2.5$. All four curves associated with different sizes cross at $W_{\mathrm{c}} = 2.1$,

suggesting a critical point of disorder induced topological transition at the thermodynamic limit, $N \to \infty$.[16,32] Although the transition at infinite size is a single point $W_c = 2.1$, we call the range $W \in (1, 2.1)$ the transition region because the Chern number plateau has collapsed for all finite sizes we calculate here. This will give rise to some finite size effects in the following. Since the main interests of this manuscript is the CC or delocalized states, our focus will be situations before the complete localization, i.e., $W < W_c$.

Now we investigate this process in the picture of CC states. In Fig. 2, we show the Chern number resolved DOS as defined in Eq. (5), which are also averaged over disorder ensembles, for different disorder strengths. From the DOS of localized states (associated with $C = 0$) in Figs. 2(a)–2(e), one can see that disorder expands both bands along the energy axis, and the bulk gap is filled gradually. In Figs. 2(f)–2(j), the DOS of delocalized states, i.e., CC states associated with $C \neq 0$ offers more information. In the clean limit, two bands possess opposite Chern numbers respectively. With increasing disorder, their centers of mass approach towards each other. Then these two opposite Chern numbers touch, merge and finally annihilate into topologically trivial states. This picture is consistent with previous studies.[16,17,32]

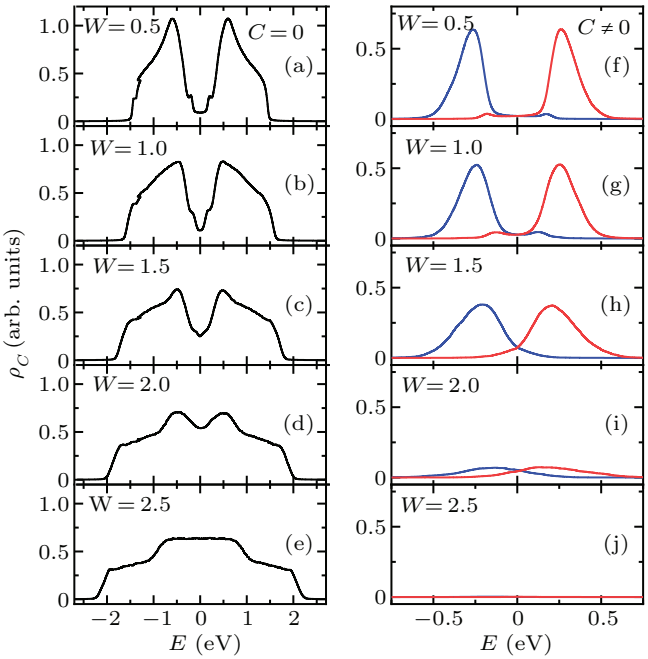


Fig. 2. Chern number resolved DOS ρ_C at different disorder strength W. The left (right) column corresponds to zero (nonzero) Chern numbers. Black, red and blue curves are for Chern numbers 0, -1 and $+1$ respectively. All data are calculated with the sample size $N = 20 \times 20$ and averaged over 1000 disorder configurations.

The above result was for a finite size sample (20×20), where the spectrum of CC states seemed to be broad and finite. Now we study their tendency during size scaling. In each dispersive band, will the CC states shrink to a single energy point in the thermodynamic limit as well?

To answer this question, we need to scrutinize the size dependence. Figure 3 presents the Chern number resolved DOS at a fixed weak disorder strength $W = 0.7$ (well before the $C = 1$ plateau collapses) with different sizes, for localized ($C = 0$) (a), and CC ($C \neq 0$) states (b), respectively. We first notice remarkably different energy scales in these two panels. This suggests that, for sufficiently large sizes, there are much more CC states than localized states. With increasing size, these two types of states exhibit different dependence on the size scaling. For the localized states [Fig. 3(a)], the DOS spectrum is almost unaffected. On the contrary, the main peaks of CC states [Fig. 3(b)] become sharper and narrower with size scaling, for both valance and conduction bands. This result implies that, although the band widths of QAH effect are finite at weak disorder, the spectrum widths of CC states still tend to be very narrow in the thermodynamic limit.

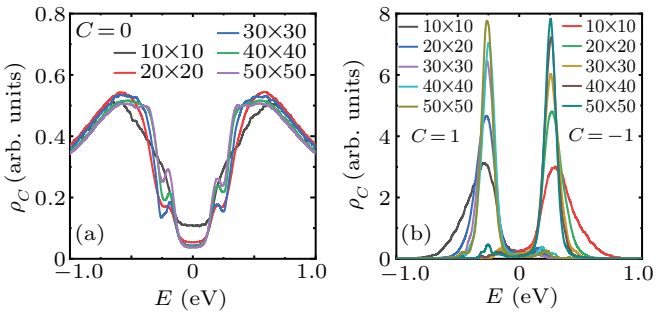


Fig. 3. Chern number resolved DOS ρ_C for different sample sizes $N_x \times N_x$, at a definite disorder strength $W = 0.7$, (a) for zero Chern number and, (b) for nonzero Chern numbers. All data are averaged over at least 100 disorder configurations.

To see this narrowing in a more quantitative way, we show the log-log plot between the spectrum width of CC states ΔE and the sample size $N \equiv N_x \times N_x$ in Figs. 4(a) and 4(b), in the Chern number plateau region $W \leq 1$, well before the disorder induced localization. For both Chern numbers, $C = \pm 1$, approximate linearities suggest that the scaling relation is a power law

$$\Delta E = N^{-x}, \tag{6}$$

where x is determined by the absolute value of the slope in this figure. This is similar to the case of IQH effect.[4] In other words, in each bulk band of a disordered QAH system, although the total band width is finite, all extended states (CC states) within this bulk band still shrink to a single energy point in the thermodynamic limit. We call this energy point of CC states as the topological center (TC) of each band. All other bulk states around the TC are localized, which will be called bulk localized states in the following, since their presence and properties do not depend on the situation of boundary conditions. Such a broad distribution of localized states is not surprising for a 2D system.[33]

This leads to a picture illustrated as follows. In a disordered QAH system at the thermodynamic limit, there is one

TC in each bulk band, with opposite-sign Chern numbers for the valence and conduction bands respectively. Since they are CC states, there will always be topological induced currents when the Fermi energy is between them. From the topological view this is not surprising because in the presence of edges, topological edge states always connect TCs with opposite Chern numbers.[24] In the bulk gap without any bulk states, they give rise to a quantized and robust Hall conductance. On the other hand, inevitably, some edge states will traverse bulk localized states around topological centers. If some of these bulk localized states are sufficiently flat, then edge states can exhibit their quantized transports in subgaps between these flat localized states. This is consistent with our previous observations in disordered 2D topological insulators,[34] where for the quantized conductance plateau, the larger portion is a topological Anderson insulator (edge states living in a mobility gap), instead of a topological band insulator (edge states living in an energy gap).

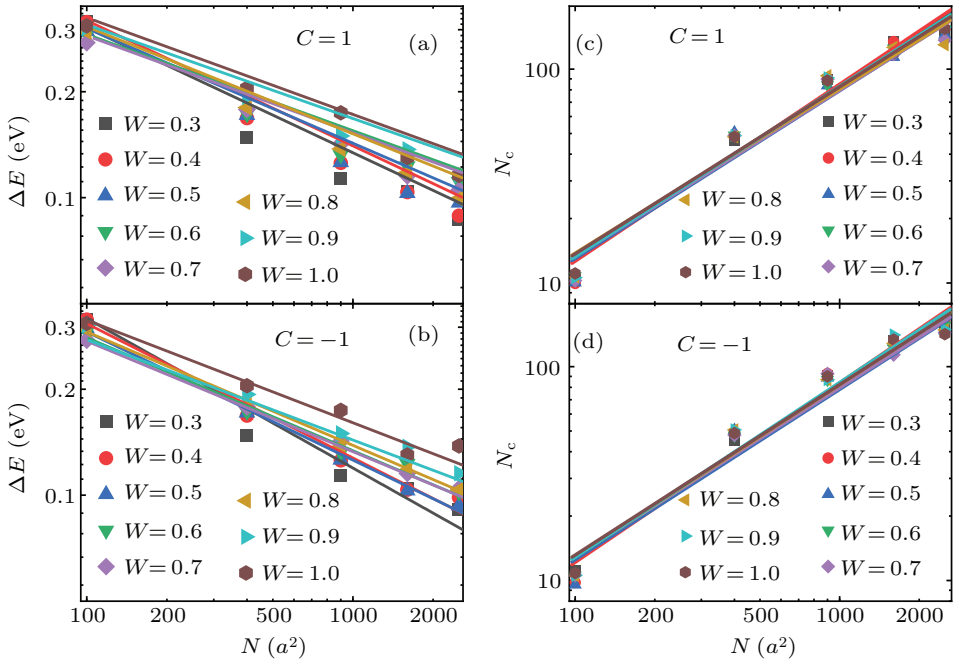


Fig. 4. Characteristic quantities of CC states as functions of sample size $N \equiv N_x \times N_x$ in double logarithm scales. (a) and (b) Spectrum width of CC DOS peak ΔE. (c) and (d) Number of CC states N_c. The upper (lower) row is for Chern number $C = 1$ ($C = -1$).

Besides the spectrum width ΔE, another aspect of CC states is their number N_c with respect to the scaling of size N. In Figs. 4(c) and 4(d), we present the log–log plot of this relation. Again, the linearities suggest a power law between them as

$$N_c = N^y, \tag{7}$$

where the exponent is determined by the slopes of lines in Figs. 5(c) and 5(d).

In Fig. 5, we present the dependence of exponents x and y (solid dotted lines) on the disorder strength W. The dependence is weak and all curves seem to be constant approximately, especially in the plateau region with weak disorder $W < 1$. We attribute the irregular fluctuations to disorders at finite sizes. At the intermediate disorder, the exponent $x \sim 0.2$, close to that found in IQH systems.[4] Moreover, the sum $x+y$ (dashed lines in Fig. 5) tends to be ~ 1.1. This was found to be 1 in IQH systems, so that the CC DOS at the TC can be finite.[4] We believe this should also be the case here in the thermodynamic limit, because we have checked that for larger sample sizes, and this sum is really closer to 1. Again, the discrepancy may come from strong disorder fluctuations and finite size effects of lattice models. For example, as one can see from Fig. 1(b), although the critical disorder strength is believed to be $W_c \sim 2.1$ in the thermodynamic limit, the averaged Chern numbers have lost their quantization after $W \sim 1.5$, for all sample sizes within our calculation capability. This will lead to remarkable finite size effects, and some subsequent statistical uncertainties exhibited in Figs. 4 and 5.

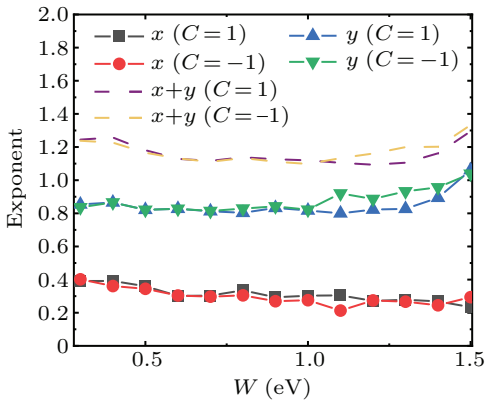


Fig. 5. Size scaling exponents of CC states with $C = \pm 1$ as functions of the disorder strength W: x defined in Eq. (6) for the spectrum width ΔE, and y defined in Eq. (7) for the number of CC states. Dashed lines are their sums $x+y$.

4. Summary

As a summary, we numerically investigate the CC states in a disordered QAH system. Performing the finite-size scaling, we conclude that within the dispersive bulk band, all CC states converge to a single energy value, similar to what happens in disorder broadened Landau levels of an IQH system. At the intermediate disorder, the shrinking rate of the spectrum width of CC states is close to that in the IQH system. This is consistent with the previous picture that the topological Anderson insulator constitutes a large portion of the quantized conductance plateau in the presence of disorder.

Appendix A: Real space representation of the BHZ model

Here we present the derivation of BHZ model of spin-up part in real space. In the momentum space, the spin-up part of the BHZ Hamiltonian reads[21]

$$\mathcal{H} = \sum_{\boldsymbol{k},\alpha\beta} c^{\dagger}_{\boldsymbol{k}\alpha} H_{\alpha\beta}(\boldsymbol{k}) c_{\boldsymbol{k}\beta}. \tag{A1}$$

The 2×2 matrix $H_{\alpha\beta}(\boldsymbol{k})$ in Eq. (A1) is

$$H(\boldsymbol{k}) = d_0(\boldsymbol{k}) I_{2\times 2} + \sum_{i=1}^{3} d_i(\boldsymbol{k})\sigma_i, \tag{A2}$$

$$\begin{aligned} d_0(\boldsymbol{k}) &= -2D\big[2-\cos(k_x)-\cos(k_y)\big], \\ d_1(\boldsymbol{k}) &= A\sin(k_x), \quad d_2(\boldsymbol{k}) = A\sin(k_y), \\ d_3(\boldsymbol{k}) &= M - 2B\big[2-\cos(k_x)-\cos(k_y)\big], \end{aligned} \tag{A3}$$

where σ_i are Pauli matrices acting on the orbital space.

Now we transform it into the real space representation by performing the inverse Fourier transform

$$c^{\dagger}_{\boldsymbol{k}\alpha} = \frac{1}{N}\sum_{\boldsymbol{r}'} \exp(-\mathrm{i}\boldsymbol{k}\cdot\boldsymbol{r}') c^{\dagger}_{\boldsymbol{r}'\alpha}, \tag{A4}$$

$$c_{\boldsymbol{k},\beta} = \frac{1}{N}\sum_{\boldsymbol{r}} \exp(\mathrm{i}\boldsymbol{k}\cdot\boldsymbol{r}) c_{\boldsymbol{r}\beta}, \tag{A5}$$

where $\boldsymbol{r}\equiv(x,y)$ is the spatial coordinate of the site, and N is total number of unit cells of the system. After inserting Eqs. (A4) and (A5) into Eq. (A1), and simplifying it by noting the orthogonal relation

$$\sum_{\boldsymbol{k}} \frac{1}{N^2} \mathrm{e}^{\mathrm{i}\boldsymbol{k}\cdot(\boldsymbol{r}-\boldsymbol{r}')} = \delta_{\boldsymbol{r},\boldsymbol{r}'}, \tag{A6}$$

we arrive at the final real space representation

$$\begin{aligned} \mathcal{H} = &\sum_{\boldsymbol{r}} c^{\dagger}_{\boldsymbol{r}} \begin{pmatrix} M-4(D+B) & 0 \\ 0 & -M-4(D-B) \end{pmatrix} c_{\boldsymbol{r}} \\ &+ \sum_{\langle \boldsymbol{r},\boldsymbol{r}+\hat{\boldsymbol{x}}\rangle} c^{\dagger}_{\boldsymbol{r}+\hat{\boldsymbol{x}}} \begin{pmatrix} D+B & -\mathrm{i}\frac{A}{2} \\ -\mathrm{i}\frac{A}{2} & D-B \end{pmatrix} c_{\boldsymbol{r}} \\ &+ \sum_{\langle \boldsymbol{r},\boldsymbol{r}+\hat{\boldsymbol{y}}\rangle} c^{\dagger}_{\boldsymbol{r}+\hat{\boldsymbol{y}}} \begin{pmatrix} D+B & \frac{A}{2} \\ -\frac{A}{2} & D-B \end{pmatrix} c_{\boldsymbol{r}}, \end{aligned} \tag{A7}$$

where $c_{\boldsymbol{r}} \equiv (c_{\boldsymbol{r}1}, c_{\boldsymbol{r}2})^{\mathrm{T}}$.

Appendix B: Numerical evaluation of Chern numbers

In this Appendix, we introduce how to associate a quantized Chern numbers to each energy level of a finite size system, based on the real space algorithm of the topological marker.[28] Consider a finite size tight-binding model with total N orbitals (and therefore N energy levels). If the Fermi level is E_n, i.e., the energy levels are occupied up to the n-th one, then the ground state projector P and its complement Q are defined as[28–30]

$$P_n = \sum_{p=1}^{n} |\psi_p\rangle\langle\psi_p|, \quad Q_n = 1 - P_n,$$

where $|\psi_p\rangle \equiv c^{\dagger}_p|0\rangle$ is the p-th single-particle energy eigenstate with eigenenergy E_p. Now the real space Chern marker can be defined to each unit cell (containing only one site here) i as

$$C_n(i) = -\frac{4}{\pi A_{\mathrm{c}}} \mathrm{Im} \sum_{\alpha\in \text{unit cell } i} \langle i\alpha|Q_n X P_n Y Q_n|i\alpha\rangle, \tag{B1}$$

where $|i\alpha\rangle \equiv c^{\dagger}_{i\alpha}|0\rangle$, X and Y are position operators in both directions respectively, and A_{c} is the area of the unit cell. For a finite size insulating sample, it has been shown that the average of $C(i)$ over its central region will converge quickly to the "real" Chern number in the process of size scaling.[29,30] In this sense, we will simply call this spatially averaged Chern marker C_n as that of the whole system when the energy levels are occupied up to E_n.

So far, the Chern number, as well as the Chern marker, is associated with the occupied states as a whole. On the other hand, the current carrying states are defined to be energy levels with nonzero Chern numbers, so one needs to associate each level with a quantized Chern number. For example, we need to investigate the density of states (DOS) from different Chern numbers separately,[4–7,31] i.e., Eq. (5).

However, for a generic Fermi level E_n of a finite size system, the ground-state Chern marker C_n may deviate from integer remarkably. This corresponds to the case that the Fermi energy is within a subband (consisting of a cluster of consecutive energy levels, which will be explained in the following) and therefore the integrated Berry curvature is not quantized.[24] As a result, a quantized Chern number can only be defined to a cluster of consecutive energy levels which constitute a physical subband, instead of to a single level. In our numerical calculations, as illustrated in Fig. B1, we first search all levels E_{n_r} ($r = 1,2,\ldots$ and $n_1 \equiv 1$) at which the ground state Chern marker C_{n_r} is well quantized, i.e., the deviation of C_{n_r} from an integer is smaller than a tolerance error ε. Then, with two adjacent quantization levels as the upper and lower band boundary respectively, a subband consisting of all levels between

them can be well defined. Consequently, a quantized Chern number can be naturally attributed to this subband. In other words, now levels with indices from $n_{r-1}+1$ to n_r constitute a subband possessing Chern number $C_{(r)} \equiv C_{n_r} - C_{n_{r-1}}$, and all these levels contribute to $\rho_{C_{(r)}}(E)$ in Eq. (5). We call these levels as "associated with Chern number C". Notice the difference between notations C_n and $C_{(r)}$. The notation C_n corresponds to the Chern marker associated with the lowest n levels, while $C_{(r)}$ corresponds to the Chern number (which has been defined to be quantized) associated with the r-th subband.

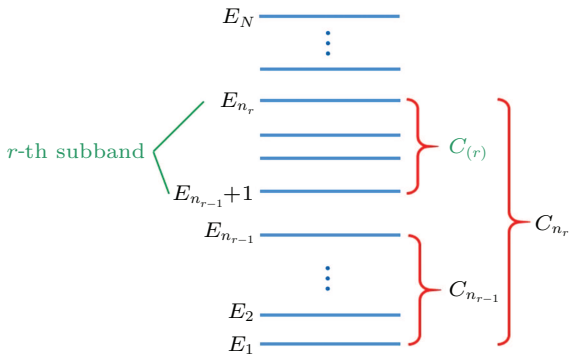


Fig. B1. Illustration of associating a quantized Chern number to discrete energy levels. All quantization levels E_{n_r} are picked out where the ground state Chern marker C_{n_r} are quantized. Then levels from $E_{n_{r-1}}+1$ to E_{n_r} are defined to be the r-th subband with a quantized Chern number $C_{(r)} \equiv C_{n_{r-1}} - C_{n_r}$.

This picture of a subband (on which a quantized Chern number can be defined) is equivalent to that defined in the momentum space of disordered supercells, with the momentum running over the disorder folded Brillioun zone.[16,35] It should be noted that, although subgaps between these subbands are finite for a certain finite-size sample, most of them will vanish after disorder average and in/or the thermodynamic limit. Only the gap survives after these two processes is a "truly" physical gap. Correspondingly, a truly physical band (which may consists of many subbands) is the set of all energy levels between two physical gaps.

Acknowledgements

This work was supported by the National Natural Science Foundation of China (Grant Nos. 11774336, 12104108, and 61427901) and the Starting Research Fund from Guangzhou University (Grant Nos. RQ2020082 and 62104360).

References

[1] Qi X L and Zhang S C 2011 *Rev. Mod. Phys.* **83** 1057
[2] Hasan M Z and Kane C L 2011 *Rev. Mod. Phys.* **82** 3045
[3] Klitzing K von, Dorda G and Pepper M 1980 *Phys. Rev. Lett.* **45** 494
[4] Huo Y and Bhatt R N 1992 *Phys. Rev. Lett.* **68** 1375
[5] Yang K and Bhatt R N 1996 *Phys. Rev. Lett.* **76** 1316
[6] Yang K and Bhatt R N 1999 *Phys. Rev. B* **59** 8144
[7] Yang K and Bhatt R N 1997 *Phys. Rev. B* **55** R1922(R)
[8] Xie X C, Wang X R and Xie X C 1998 *Phys. Rev. Lett.* **80** 3563
[9] Furusaki A 1999 *Phys. Rev. Lett.* **82** 604
[10] Haldane F D M 1988 *Phys. Rev. Lett.* **61** 2015
[11] Liu C X Liu, Qi X L, Dai X, Fang Z and Zhang S C 2008 *Phys. Rev. Lett.* **101** 146802
[12] Chang C Z, Zhang J, Feng X, Shen J, Zhang Z, Guo M, Li K, Ou Y, Wei P, Wang L L, Ji Z Q, Feng Y, Ji S, Chen X, Jia J, Dai X, Fang Z, Zhang S C, He K, Wang Y, Lu L, Ma X C and Xue Q K 2013 *Science* **340** 167
[13] Bestwick A J, Fox E J, Kou X, Pan L, Wang K L and Goldhaber-Gordon D 2015 *Phys. Rev. Lett.* **114** 187201
[14] Wang S W, Xiao D, Dou Z, Cao M, Zhao Y F, Samarth N, Chang C Z, Connolly M R and Smith C G 2020 *Phys. Rev. Lett.* **125** 126801
[15] Li Z and Wang Z F 2020 *Chin. Phys. B* **29** 107101
[16] Zhang Y Y, Chu R L, Zhang F C and Shen S Q 2012 *Phys. Rev. B* **85** 035107
[17] Song Z G, Zhang Y Y, Song J T and Li S S 2016 *Sci. Rep.* **10** 19018
[18] Wang S S, Zhang Y Y, Guan J H, Yu Y, Xia Y and Li S S 2019 *Phys. Rev. B* **99** 125414
[19] Li H, Chen C Z, Jiang H and Xie X C 2021 *Phys. Rev. Lett.* **127** 236402
[20] Zhang Z Q, Chen C Z, Wu Y, Jiang H, Liu J, Sun Q F and Xie X C 2021 *Phys. Rev. B* **103** 075434
[21] Bernevig A, Hughes T and Zhang S C 2006 *Science* **314** 1757
[22] Qi X L, Wu Y S and Zhang S C 2006 *Phys. Rev. B* **74** 085308
[23] Boyers E, Crowley P J D, Chandran A and Sushkov A O 2020 *Phys. Rev. Lett.* **125** 160505
[24] Xiao D, Chang M C and Niu Q 2010 *Rev. Mod. Phys.* **82** 1959
[25] Halperin B I 1982 *Phys. Rev. B* **25** 2185
[26] He Y, Jiang Y, Zhang T, Huang H, Fang C and Jin Z 2019 *Chin. Phys. B* **28** 087102
[27] Liu J S, Han Y Z and Liu C S 2020 *Chin. Phys. B* **29** 010302
[28] Bianco R and Resta R 2011 *Phys. Rev. B* **84** 241106(R)
[29] Bianco R and Resta R 2013 *Phys. Rev. Lett.* **110** 087202
[30] Marrazzo A and Resta R 2017 *Phys. Rev. B* **95** 121114
[31] Ippoliti M and Bhatt R N 2020 *Phys. Rev. Lett.* **124** 086602
[32] Qiao Z, Han Y, Zhang L, Wang K, Deng X and Jiang H 2016 *Phys. Rev. Lett.* **117** 056802
[33] Abrahams E, Anderson P W, Licciardello D C and Ramakrishnan T V 1979 *Phys. Rev. Lett.* **42** 673
[34] Zhang Y Y and Shen S Q 2013 *Phys. Rev. B* **88** 195145
[35] Essin A M and Moore J E 2007 *Phys. Rev. B* **76** 165307